ELSEVIER

Composites: Part B 30 (1999) 603–612

composites
Part B: engineering

www.elsevier.com/locate/compositesb

Modeling of smart composite box beams with nonlinear induced strain

A. Chattopadhyay*, H. Gu, Q. Liu

Department of Mechanical and Aerospace Engineering, Arizona State University, Tempe, AZ 85287-6106, USA

Received 18 September 1998; accepted 15 March 1999

Abstract

A new smart composite box beam model is developed to investigate the behavior of helicopter rotor blades built around the active box beam. Piezoelectric actuators and sensors are surface bonded on the walls of the composite box beam. The new theory, based on a refined higher order displacement field of a plate with eccentricity, is a three-dimensional model which approximates the elasticity solution so that the box beam cross-sectional properties are not reduced to one-dimensional beam parameters. Both in-plane and out-of-plane warpings are included automatically in the formulation. The formulations also include nonlinear induced strain effects of piezoelectric actuators. The procedure is implemented using finite element method. The developed theory is used to model the load carrying member of helicopter rotor blades with moderately thick-walled sections. Static analysis of the smart box beam under varying degrees of actuation has been performed. Very good overall agreement is observed with available experimental data for thin-walled sections without embedded actuators. The results show that piezoelectric actuation significantly reduces the deflection along the box beam span and therefore can be used to control the magnitude of rotor blade vibrations. The nonlinear actuation effect is found to be closely related to the material stiffness of the primary structure.

Keywords: A. Smart materials; Box beam

1. Introduction

Recent research has shown that improvement in helicopter vibration can be achieved through the implementation of active control technology using smart materials. Smart composite structures have received considerable attention due to the potential for designing adaptive structures that are both light in weight and possess adaptive control capabilities. Due to the high strength-to-weight ratio offered by composites, structural weight is much less of an issue compared to isotropic materials. Therefore it is no longer necessary to use thin-walled sections to model the load-carrying sections. For example, thick composite spars are currently being used to model the principal load carrying element in the Advanced Technology Blades (ATB) [1] used in the XV-15 tilt rotor aircraft. The classical theories are no longer adequate for modeling such sections. Also, the incorporation of smart materials into the primary structure introduces additional discontinuities that require careful modeling. Thus, it is essential to develop a general framework for the comprehensive analysis of such smart composite structural elements of arbitrary wall thickness and embedded and/or surface bonded actuators.

Beam theories associated with isotropic materials have been well understood for years [2]. Recently, several composite beam theories [3–6] have been reported. The more comprehensive anisotropic theories rely on a full three-dimensional (3D) finite element solution that can become very computationally intensive [4,5]. A comprehensive modeling of beams with solid cross sections was also presented using a full 3D finite element solution technique [7]. The variational asymptotic approach was used to model beams of arbitrary cross sections [3], which includes warping terms. In the variational asymptotic approach [8], the 3D properties of the beam are reduced to 1D beam properties (extension, twist and two bending terms) and the beam response is then approximated based on a 1D analysis. The theory does include both in-plane and out-of-plane warping effects. In other analysis of closed sections [6,9,10] as well as in some of the 3D finite element models [5], the classical laminate theory is used to model the individual plate elements of each beam. The theory, which neglects transverse shear effects, is only appropriate for thin laminates. However, in case of anisotropic material, the changes in interlamina stiffnesses lead to nonnegligible transverse shear deformation even for "so-called" thin laminates [11–13].

* Corresponding author. Tel.: + 1-480-965-9342; fax: + 1-480-965-1384.

E-mail address: chattopa@enws148.eas.asu.edu (A. Chattopadhyay)

1359-8368/99/$ - see front matter
PII: S1359-8368(99)00019-0

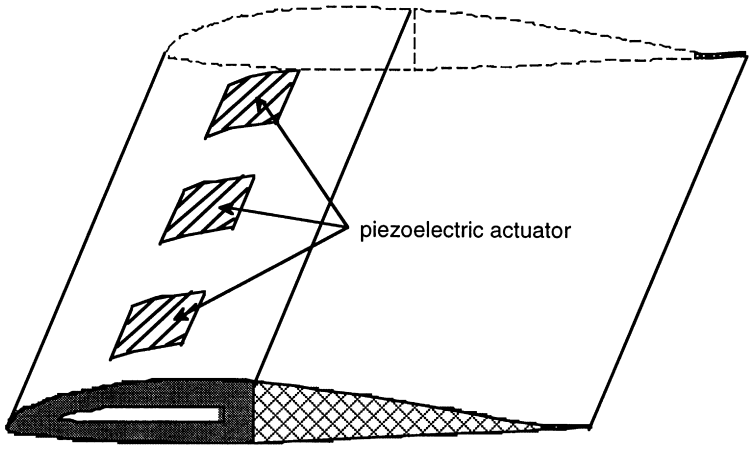

Fig. 1. Rotary wing with piezoelectric actuators.

The static and dynamic responses of composite beam and rotor blades with surface bonded piezoceramic actuators were reported by Chandra [14] and Park and Chopra [15]. A smart composite beam model was developed to represent the load carrying structure using strain theory. The individual blade control of vibration reduction using a smart blade structure was also studied by Nitzsche [16]. Recently, Chen and Chopra [17,18] investigated an alternate scheme of distributed piezo actuators to actively twist the blade. In their work, a 1D uniform strain theory was used to predict the static response. Later, Chen and Chopra [19] refined the 1D uniform strain theory to include closely spaced actuator interaction effects, based on block-force assumption, and developed a Bernoulli–Euler plate theory to predict the static response of smart composite beams. However, the structural analysis used in their work were based on a single solid beam approach. Such an approach cannot accurately represent real rotary wing load-carrying structures.

A study of vibratory loads reduction of rotor blades using piezoelectric materials is presented. A new smart composite box beam model is developed to investigate vibration control of helicopter rotor blades built around the active box beam. The mechanical behavior of the composite box beam with surface bonded and embedded piezoelectric actuators and sensors is studied in detail. A previously developed higher order theory based composite box beam approach [20] is modified to model rectangular box beams, of arbitrary wall thickness, with surface bonded piezoelectric actuators. Further, refinements are also made to the theory to take into account the effect of eccentricities in plate theory caused by the presence of surface bonded actuators. The theory, which is based on a refined displacement field, is a 3D model which approximates the elasticity solution so that the beam cross-sectional properties are not reduced to 1D beam parameters. Both in-plane and out-of-plane warping are included automatically in the formulation. The developed model satisfies the stress free boundary conditions at the inner and outer surfaces of the beam. Continuities in displacements are also ensured at the interface between the composite laminate and the embedded piezoelectric actuators. The analytical model is implemented using the finite element technique. Since the relationships between the induced strain due to actuation and the applied electric field are nonlinear in nature [21], formulation presented in the current research includes these nonlinear induced strain effects.

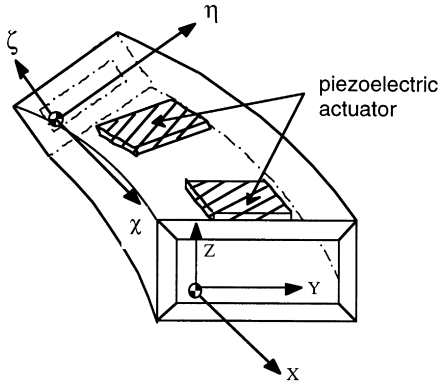

Fig. 2. Composite box beam.

2. Higher order theory based formulation

A single-celled composite box beam of arbitrary wall thickness is used to model the principal load-carrying element in the rotor blade (Fig. 1). The piezoelectric actuators and sensors are surface bonded to the top and bottom surfaces of the box beam. The box beam is modeled using composite laminates representing the four walls (Fig. 2). Since the neutral plane in the box beam structure does not coincide with the mid-plane of the plate, the eccentricity between the neutral plane of the box beam and the middle plane of the individual plate must be taken into account in formulating the stiffness of the smart box beam. Therefore, a general higher order displacement field is developed to model the individual composite walls with eccentricity.

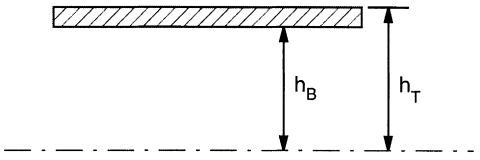

Fig. 3. Modeling composite plate with eccentricity.

The in plane displacements are assumed to be effectively expressed by a cubic function through the thickness (z) and the transverse displacement is assumed to be independent of z. To model such structures, the general displacement field is defined as

$$u_1(\chi,\eta,\zeta) = u_0(\chi,\eta) - \zeta\frac{\partial u_3(\chi,\eta)}{\partial\chi} + \zeta\psi_\chi(\chi,\eta) + \zeta^2\phi_\chi(\chi,\eta) + \zeta^3\varphi_\chi(\chi,\eta)$$

$$u_2(\chi,\eta,\zeta) = v_0(\chi,\eta) - \zeta\frac{\partial u_3(\chi,\eta)}{\partial\eta} + \zeta\psi_\eta(\chi,\eta) + \zeta^2\phi_\eta(\chi,\eta) + \zeta^3\varphi_\eta(\chi,\eta)$$

$$u_3(\chi,\eta,\zeta) = w_0(\chi,\eta) \tag{1}$$

where, u_1, u_2 and u_3 are the in-plane and out-of-plane displacements at a point (χ,η,ζ), u_0, v_0 and w_0 represent the displacements at the mid-plane, ψ_χ and ψ_η represent the rotations of the normals to the mid-plane and ϕ_χ, ϕ_η, φ_χ and φ_η are the higher order terms. The higher order functions are determined based on the condition that the transverse shear stresses, $\sigma_{\chi\zeta}$ and $\sigma_{\eta\zeta}$, vanish on the inner and outer surfaces (Fig. 3) of the beam.

$$\sigma_{\chi\zeta}(\chi,\eta,\zeta=h_T) = 0, \qquad \sigma_{\eta\zeta}(\chi,\eta,\zeta=h_T) = 0$$

$$\sigma_{\chi\zeta}(\chi,\eta,\zeta=h_B) = 0, \qquad \sigma_{\eta\zeta}(\chi,\eta,\zeta=h_B) = 0. \tag{2}$$

For composite laminates made up of layers of orthotropic lamina, this is equivalent to the requirement that the corresponding strains be zero on these surfaces:

$$\varepsilon_{\chi\zeta}(\chi,\eta,\zeta=h_T \text{ or } h_B) = \frac{\partial u_1}{\partial\zeta} + \frac{\partial u_3}{\partial\chi} = \psi_\chi + 2\zeta\phi_\chi + 3\zeta^2\varphi_\chi = 0$$

$$\varepsilon_{\eta\zeta}(\chi,\eta,\zeta=h_T \text{ or } h_B) = \frac{\partial u_2}{\partial\zeta} + \frac{\partial u_3}{\partial\eta} = \psi_\eta + 2\zeta\phi_\eta + 3\zeta^2\varphi_\eta = 0. \tag{3}$$

From Eq. (3), the higher order terms can be expressed by the lower order terms:

$$\phi_\chi = -\frac{h_T + h_B}{2h_Th_B}\psi_\chi, \qquad \varphi_\chi = \frac{1}{3h_Th_B}\psi_\chi$$

$$\phi_\eta = -\frac{h_T + h_B}{2h_Th_B}\psi_\eta, \qquad \varphi_\eta = \frac{1}{3h_Th_B}\psi_\eta. \tag{4}$$

Using Eq. (4), it can be shown that the original displacement field (Eq. (1)) is reduced to the following refined displacement field:

$$u_1(\chi,\eta,\zeta) = u_0(\chi,\eta) + \zeta\left[\psi_\chi(\chi,\eta) - \frac{\partial w_0(\chi,\eta)}{\partial\chi}\right] - \frac{\zeta^2}{2}\frac{h_T + h_B}{h_Th_B}\psi_\chi(\chi,\eta) + \frac{\zeta^2}{3h_Th_B}\psi_\chi(\chi,\eta)$$

$$u_2(\chi,\eta,\zeta) = v_0(\chi,\eta) + \zeta\left[\psi_\eta(\chi,\eta) - \frac{\partial w_0(\chi,\eta)}{\partial\eta}\right] - \frac{\zeta^2}{2}\frac{h_T + h_B}{h_Th_B}\psi_\eta(\chi,\eta) + \frac{\zeta^2}{3h_Th_B}\psi_\eta(\chi,\eta)$$

$$u_3(\chi,\eta,\zeta) = w_0(\chi,\eta). \tag{5}$$

For an orthotropic composite plate with piezoelectric layers, the constitutive relationships can be written as

$$\boldsymbol{\sigma} = \bar{\mathbf{Q}}(\boldsymbol{\varepsilon} - \boldsymbol{\Lambda}) \tag{6}$$

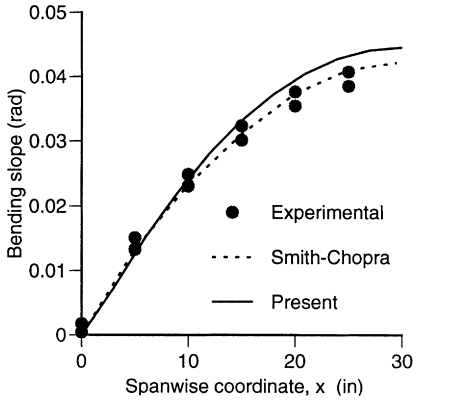

Fig. 4. Variation of bending slope of thin-walled box beam under 1 lb tip bending load.

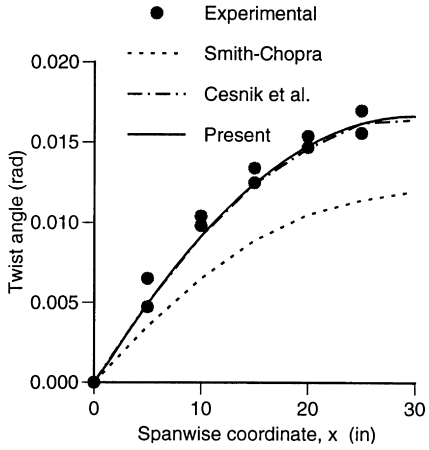

Fig. 5. Variation of twist angle of thin-walled box beam under 1 lb tip bending load.

where $\mathbf{Q}$ is the elastic stiffness matrix, $\boldsymbol{\varepsilon}$ and $\boldsymbol{\sigma}$ are the strain and stress vectors, respectively and $\boldsymbol{\Lambda}$ is the induced strain vector.

3. Nonlinear induced strain

The electro-mechanical coupling between the applied electric field, $\mathbf{E}$, and the induced strain, $\boldsymbol{\Lambda}$, in the piezoelectric material is governed by the coupling coefficient matrix, $\mathbf{d}$, which represent piezoelectric material properties. The behavior of piezoelectric actuators under high applied voltage was studied by Tiersten using a theory linear in displacement gradients but cubic in electric field [22]. In the current study, the experimental results of Crawley and Lazarus [21] was used to model the nonlinear effect. According to this study, the coupling coefficients depend on the actual strain in the actuator as well. That is

$$\boldsymbol{\Lambda} = \mathbf{d}^{\mathrm{T}}(\boldsymbol{\varepsilon})\mathbf{E} = (\mathbf{d}_0^{\mathrm{T}} + \boldsymbol{\varepsilon}^{*}\mathbf{d}_1^{\mathrm{T}} + \boldsymbol{\varepsilon}^{*\mathrm{T}}\boldsymbol{\varepsilon}^{*}\mathbf{d}_2^{\mathrm{T}} + \cdots)\mathbf{E} \tag{7}$$

However, due to the weak nonlinearity, they can be rewritten using first order Taylor series expansion without loss of the accuracy.

$$\boldsymbol{\Lambda} \cong (\mathbf{d}_0^{\mathrm{T}} + \boldsymbol{\varepsilon}^{*}\mathbf{d}_1^{\mathrm{T}})\mathbf{E}. \tag{8}$$

The coefficients contained in $\mathbf{d}_0$ and $\mathbf{d}_1$ can be identified using functional relationships of the strain versus electric field obtained from experimental data of an unconstrained piezoelectric actuator, and the details of the strain matrix $\boldsymbol{\varepsilon}^{*}$ is given in the Appendix. The benefit of using the current nonlinear induced strain formulation, as shown in Eq. (8), is that the final governing equations remain linear.

4. Finite element modeling

The finite element method (FEM) is used to implement the refined higher order theory since it allows for the analysis of practical geometry and boundary conditions. The finite element equations are derived using the variational principle, which is stated as follows:

$$\begin{aligned}\delta\Pi &= \int_{\mathbf{z}}\int_{\boldsymbol{\Omega}} \delta\boldsymbol{\varepsilon}^{\mathrm{T}}\boldsymbol{\sigma}\,\mathrm{d}\boldsymbol{\Omega}\,\mathrm{d}\mathbf{z} - \int_{\boldsymbol{\Omega}} \delta\mathbf{u}^{\mathrm{T}}\mathbf{q}\,\mathrm{d}\boldsymbol{\Omega} \\ &= \int_{\mathbf{z}}\int_{\boldsymbol{\Omega}} \delta\boldsymbol{\varepsilon}^{\mathrm{T}}\bar{\mathbf{Q}}(\boldsymbol{\varepsilon} - \boldsymbol{\Lambda})\,\mathrm{d}\boldsymbol{\Omega}\,\mathrm{d}\mathbf{z} - \int_{\boldsymbol{\Omega}} \delta\mathbf{u}^{\mathrm{T}}\mathbf{q}\,\mathrm{d}\boldsymbol{\Omega} = 0\end{aligned} \tag{9}$$

where $\boldsymbol{\Omega}$ is integration area of box beam and $\mathbf{q}$ is the applied load vector. To discretize the smart box beam structure, cubic Hermit interpolation function is used for the three translation displacement components, u_0, v_0 and w_0. For the two rotational components, ψ_χ and ψ_η, linear interpolation function is employed. Here, these interpolation functions are combined into one interpolation matrix, $\mathbf{N}$, and the matrix form of the discretization is stated as follows:

$$\begin{aligned}&\mathbf{u} = \mathbf{N}\mathbf{u}_0, \qquad \boldsymbol{\varepsilon} = \mathbf{L}\mathbf{N}\mathbf{u}_0 = \left(\sum_{i=0}^{3}\mathbf{z}^i\mathbf{B}_i\right)\mathbf{u}_0, \\ &\mathbf{D}_i = \int_{\mathbf{z}}\mathbf{z}^i\bar{\mathbf{Q}}\,\mathrm{d}\mathbf{z}\end{aligned} \tag{10}$$

with

$$\mathbf{B} = \mathbf{L}\mathbf{N} = \left(\sum_{i=0}^{3}\mathbf{z}^i\mathbf{L}_i\right)\mathbf{N}, \qquad \mathbf{B}_i = \mathbf{L}_i\mathbf{N}. \tag{11}$$

Using Eq. (10), the discretized form of variational principle, Eq. (9), can be expressed as follows:

$$\begin{aligned}&\delta\mathbf{u}_0^{\mathrm{T}}\left[\int_{\boldsymbol{\Omega}}\left(\sum_{i=0}^{6}\sum_{j=0}^{i}\mathbf{B}_j^{\mathrm{T}}\mathbf{D}_i(\mathbf{I} - \mathbf{d}_1\mathbf{E})\mathbf{B}_{i-j}\right)\mathrm{d}\boldsymbol{\Omega}\mathbf{u}_0\right. \\ &\left. - \int_{\boldsymbol{\Omega}}\sum_{i=0}^{3}\mathbf{B}_i^{\mathrm{T}}\mathbf{D}_i\mathbf{d}_0\mathbf{E}\,\mathrm{d}\boldsymbol{\Omega} - \int_{\boldsymbol{\Omega}}\mathbf{q}\,\mathrm{d}\boldsymbol{\Omega}\right] \\ &= 0.\end{aligned} \tag{12}$$

Therefore, the global finite element equations are then written as

$$(\mathbf{K} - \mathbf{K}_{\mathrm{n}})\mathbf{u}_0 = \mathbf{f} + \mathbf{f}_{\mathrm{p}} \tag{13}$$

with

$$\mathbf{K} = \int_{\boldsymbol{\Omega}}\left(\sum_{i=0}^{6}\sum_{j=0}^{i}\mathbf{B}_j^{\mathrm{T}}\mathbf{D}_i\mathbf{B}_{i-j}\right)\mathrm{d}\boldsymbol{\Omega}$$

$$\mathbf{K}_{\mathrm{n}} = \int_{\boldsymbol{\Omega}}\left(\sum_{i=0}^{6}\sum_{j=0}^{i}\mathbf{B}_j^{\mathrm{T}}\mathbf{D}_i\mathbf{d}_1\mathbf{E}\mathbf{B}_{i-j}\right)\mathrm{d}\boldsymbol{\Omega}$$

$$\mathbf{f}_{\mathrm{p}} = \int_{\boldsymbol{\Omega}}\sum_{i=0}^{3}\mathbf{B}_i^{\mathrm{T}}\mathbf{D}_i\mathbf{d}_0\mathbf{E}\,\mathrm{d}\boldsymbol{\Omega}, \qquad \mathbf{f} = \int_{\boldsymbol{\Omega}}\mathbf{q}\,\mathrm{d}\boldsymbol{\Omega} \tag{14}$$

where the quantities $\mathbf{K}$, $\mathbf{F}$ and $\mathbf{u}$ denote the regular stiffness matrix, the force vector due to a distributed load and the nodal displacement vector, respectively. The quantity $\mathbf{K}_{\mathrm{n}}$ represents the additional stiffness matrix due to the nonlinear part of induced strain and $\mathbf{F}_{\mathrm{p}}$ is the force vector due to linear part of piezoelectric actuation. It can be seen from Eq. (12) that the nonlinear component of induced strain affects the structural stiffness through the introduction of the additional stiffness components.

5. Results and discussion

A correlation with available thin-walled composite box beam data is presented first to illustrate the accuracy of the model. Next, numerical results are presented for a rotor blade built around the active box beam with surface bonded

Table 1
Details of experimental beam

Length	30 in.
Width	0.953 in.
Depth	0.53 in.
Ply thickness	0.005 in.
Number of plies	6
Total wall thickness	0.030 in.
E_1	20.59×10^6 psi
E_2	1.42×10^6 psi
G_{12}	0.89×10^6 psi
G_{13}	0.70×10^6 psi
ν_{12}	0.42
Horizontal wall lay-up	$[45°]_6$
Vertical wall lay-up	$[45°/-45°]_3$

piezoelectric actuator pairs subjected to a static distributed load.

To validate the developed procedure, comparisons are made with experimental results of a thin-walled box beam [9] and a previously developed analytical model [10]. The analytical model developed by Smith and Chopra [10] is a 1D thin-walled beam model, based on the Classical Laminate Theory, in which the out of plane warping effects are based on a contour analysis. The details of the beam studied are presented in Table 1, where E is the Young's modulus and ν is the Poisson's ratio. Figs. 4 and 5 present the bending slope and the induced twist, respectively, for a 1 lb vertical load at the tip. Very good agreement is observed between the results obtained using the present theory and the experimental data in most cases. It is also seen that results predicted in Ref. [9] are significantly lower than the experimental data, particularly for the induced twist due to vertical tip load (Fig. 5). Further, the current results are in excellent agreement with those obtained using the variational asymptotical approach [23] well suited for this thin-walled box beam.

Further validation is performed for a symmetric 45° thick-walled box beam (Table 1) using the NASTRAN results due to the lack of available experimental data. The thick-walled

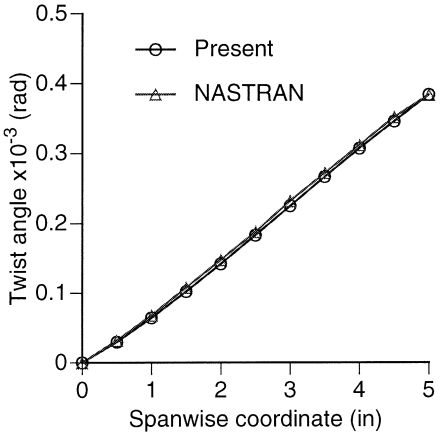

Fig. 6. Variation of twist angle of thick-walled box beam under 100 lb tip bending load.

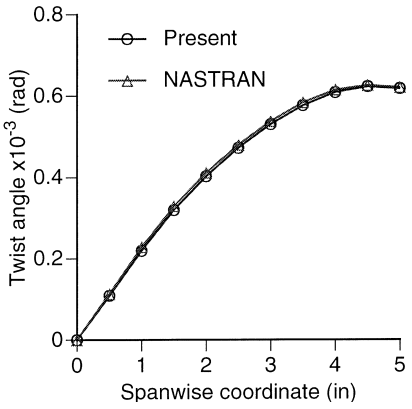

Fig. 7. Variation of twist angle of thick-walled box beam under 100 lb in. tip moment.

beam configuration represents a typical example of thick composite load carrying member with transverse shear effects. The beams studied have a length-to-width ratio (L/c) of 2.5 and a width-to-height ratio (c/d) of 2. The wall thickness is selected in this study as 0.25 in. resulting in the values of the width-to-thickness ratio, $c/h = 8$, in the horizontal walls and the height-to-thickness ratio, $d/h = 4$, in the vertical walls. This beam configuration is subjected to a 100 lb bending load at the tip as well as a 100 lb in. tip moment. Figs. 6 and 7 present the elastic twist for the thick-walled beam in both load cases, obtained using the present model and NASTRAN analysis. The NASTRAN results are obtained using QUAD4 plate elements based on first-order shear deformation theory. Very good correlation is observed between the present approach and NASTRAN analysis. This indicates that the present model is able to accurately capture the significant transverse shear effects present in the thick-walled composite box beam.

Next, parametric studies are conducted to investigate the optimal placement of a pair of piezoelectric actuators with dimensions, $10 \times 6.5 \times 0.02$ in., located at the top and bottom surfaces, by varying their spanwise locations (Fig. 8). Graphite/epoxy material is used for the composite box beam (properties listed in Table 2). As seen from Fig. 9, due to piezoelectric actuation, the percentage reductions in all three tip deformation (flap, lag and twist) generally increase as the actuator approaches the fixed end. However, when the actuators are placed very near to the fixed end, there is sudden increase in both lag deflection and twist angle. The maximum reductions in the flap and lag deflections and the twist angle, measured at the box beam tip, are about 20, 18 and 15%, respectively. The observation support the fact that the best location of the actuators, along the cantilever box beam span, is near the fixed end, where the largest control authority is expected.

To calculate the actuation capability, results are presented for the Graphite/epoxy box beam covered by a layer of piezoelectric actuators at the top and the bottom surfaces (Figs. 10–12). The values of the flap deflection (Fig. 10), the lag deflection (Fig. 11) and the twist angle (Fig. 12) decrease

Table 2
Material properties of smart box beam

	E_1 (gsi)	E_2 (gsi)	ν_{12}	G_{12}, G_{13} (gsi)	G_{23} (gsi)	d_L ($\times 10^{-9}$ in/V)	d_0 ($\times 10^{-9}$ in/V)	d_1 ($\times 10^{-5}$ in/V)
Graphite/epoxy	25	1	0.33	0.5	0.2			
Glass/epoxy	5.67	1.6	0.3	0.58	0.28			
PZT	9.14	9.14	0.33	3.51	3.51	9.921	9.724	3.299

substantially with increase in the electric voltage. At actuation of 400 V, the flap and the lag deflection and the twist angle at the box beam tip reduce by about 75, 80 and 98%, respectively, compared to the case without actuation. Due to the discrete nature of the actuators, two cases of the smart box beam with discretely located actuators are also presented (Figs. 13–15). Eight pairs of actuators are placed consecutively near the fixed end in Case 1 and they are assumed to be located evenly along the box beam span in Case 2. Once again, the box beam deformation reduces with increase in the voltage. However, the magnitude of reduction is more significant in Case 1 (actuators are near fixed end) compared to that in Case 2 (actuators are evenly located along the span). As observed from Figs. 13–15, the reductions in flap deflection (Fig. 13), lag deflection (Fig. 14) and twist angle (Fig. 15) in Case 1 under the actuation of 200 V is even larger than the corresponding reductions obtained in Case 2 under 400 V. This means that the most effective location of actuators is near the fixed end of the cantilever box beam, irrespective of the number of actuator pairs that are used. The presence of the actuators alters the box beam stiffness. Therefore, the discontinuity observed in the slope of the twist angle, as shown in Figs. 14 and 15, is due to the sudden change in spanwise stiffness of the smart box beam at discrete actuator location.

To investigate the effects of composite parameter variations on the smart composite box beam, two cases with different ply stacking sequence of $[90°/45°/-45°/90°]_S$ and $[0°/45°/-45°/90°]_S$ are studied. It is assumed that the same ply stacking sequence is applied to four walls and two pairs of piezoelectric actuators are located at the clamped end and the middle of the box beam, respectively. The flap, lag and twist deformations are presented in Figs. 16–18, for both ply stacking sequence cases, without and with active control (200 V). As seen from these figures, the percentage

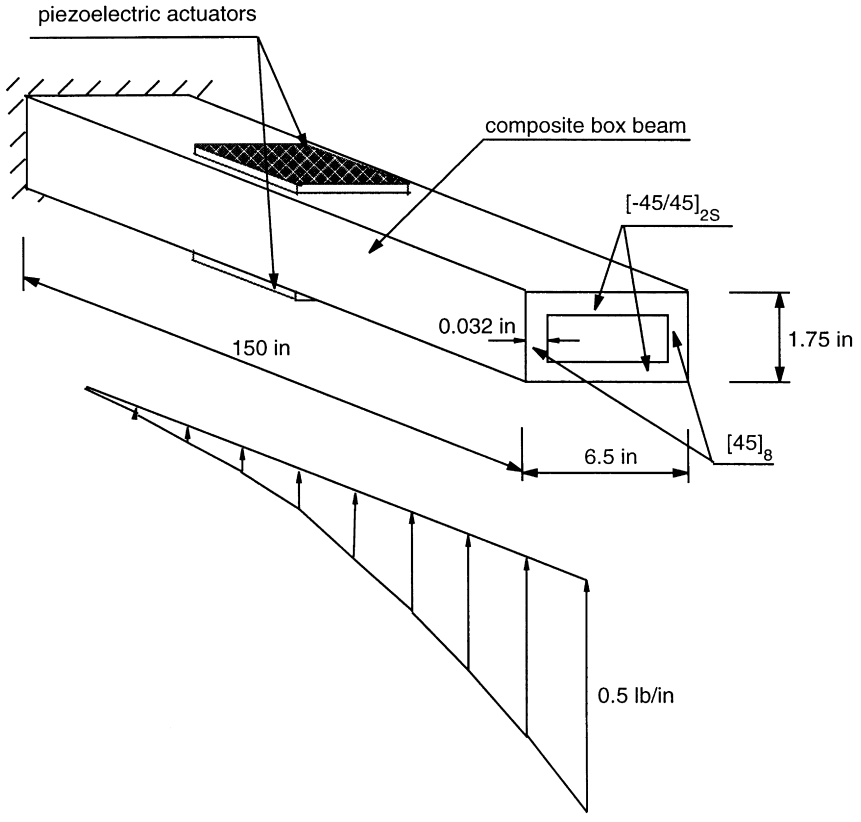

Fig. 8. Composite box beam configuration.

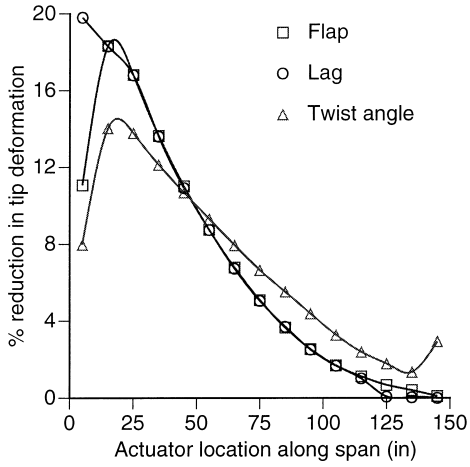

Fig. 9. Effect of actuator location.

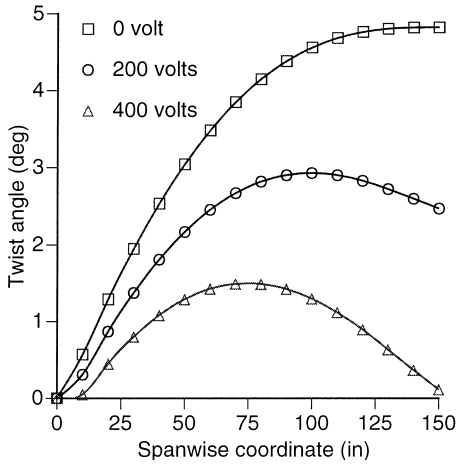

Fig. 12. Twist angle of box beam bonded by 15 pairs of actuators at top and bottom surfaces.

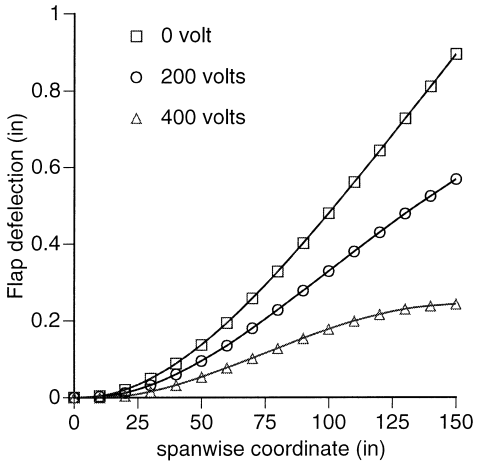

Fig. 10. Flap deflection of box beam bonded by 15 pairs of actuators at top and bottom surfaces.

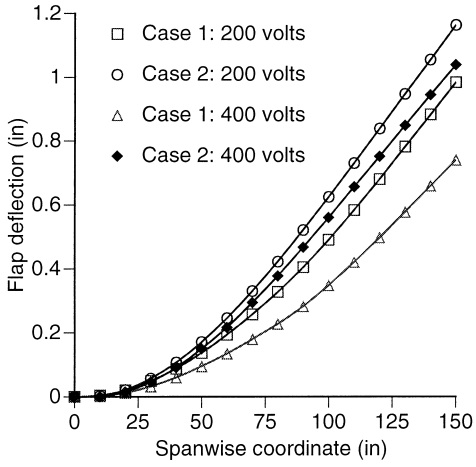

Fig. 13. Flap deflection of box beam bonded by 8 pairs of actuators at top and bottom surfaces (Case 1: actuators placed near the clamped end; Case 2: actuators placed evenly along the span).

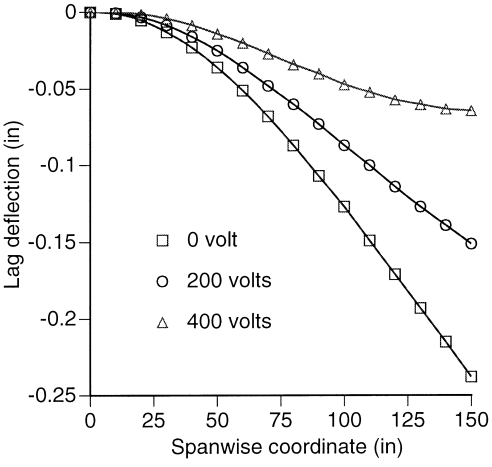

Fig. 11. Leg deflection of box beam bonded by 15 pairs of actuators at top and bottom surfaces.

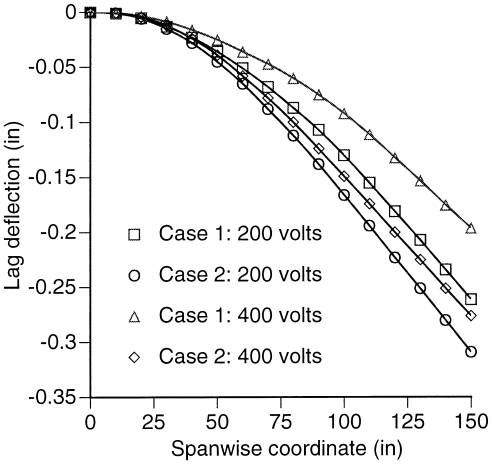

Fig. 14. Leg deflection of box beam bonded by 8 pairs of actuators at top and bottom surfaces (Case 1: actuators placed near the clamped end; Case 2: actuators placed evenly along the span).

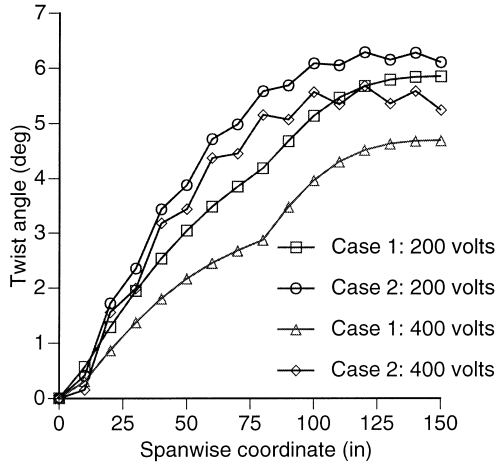

Fig. 15. Twist angle of box beam bonded by 8 pairs of actuators at top and bottom surfaces (Case 1: actuators placed near the clamped end; Case 2: actuators placed evenly along the span).

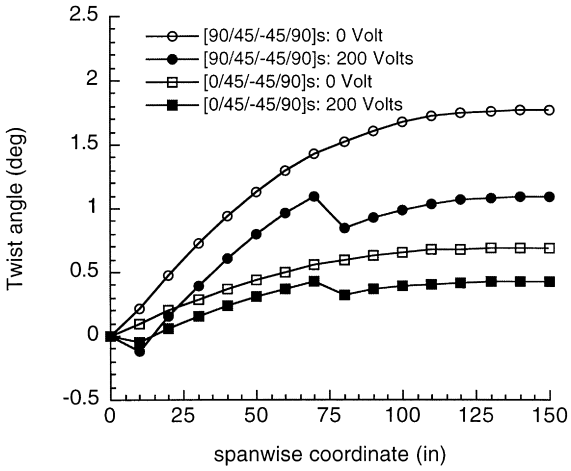

Fig. 18. Twist angle of box beam with ply stacking sequence of $[90°/45°/-45°/90°]_S$ and $[0°/45°/-45°/90°]_S$.

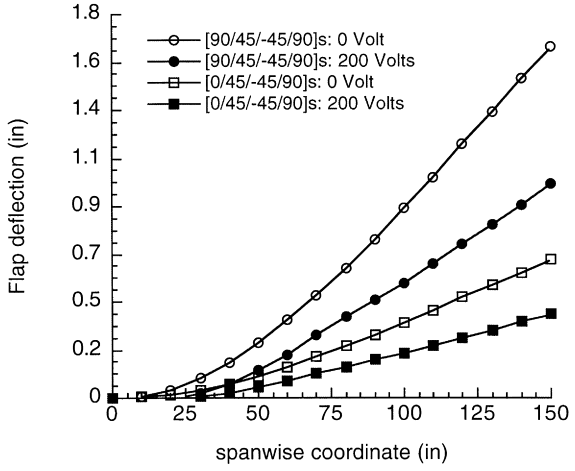

Fig. 16. Flap deflection of box beam with ply stacking sequences of $[90°/45°/-45°/90°]_S$ and $[0°/45°/-45°/90°]_S$.

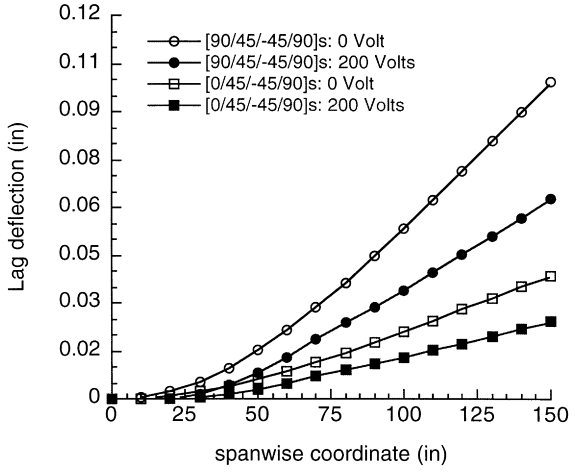

Fig. 17. Lag deflection of box beam with ply stacking sequences of $[90°/45°/-45°/90°]_S$ and $[0°/45°/-45°/90°]_S$.

reductions in all three deformations are about the same (about 40%) for both cases with active control. This implies that stiffness changes in the box beam will not have much effect on the active control authority using piezoelectric actuators. Once again, the discontinuity in slope of the twist angle is observed in Fig. 18 at discrete actuator location.

It must be noted that since the stiffness of the box beam structure is substantially higher than that of a plate structure, more powerful piezoelectric actuators are required to effectively control such structure. The theory and the finite element model developed in this research is expected to serve as an accurate analysis tool for thick-walled composite box beam structures controlled by piezoelectric actuators within the theory of piezoelectro-elasticity. The issue of the applied voltage which current piezoelectric actuators can withstand was not considered critical since research on advanced piezoelectric actuators is still on going. New actuators that can withstand higher voltage will be practical in the near future. Therefore, results are presented for a high voltage case (400 V) to examine the potential control authority for future helicopter blade design.

Finally, the nonlinear induced strain effect on smart composite beams is considered. The static response under actuation only is analyzed and it is assumed that all of the beam surfaces are covered with piezoelectric actuators. Comparisons of box beam flap deflections with and without nonlinear induced strain effect are presented in Figs. 19 and 20 for graphite/epoxy and glass/epoxy, respectively. Less than 4% deviation is observed for the graphite/epoxy box beam with higher stiffness as shown in Fig. 19. However, significant deviation (about 10%) is obtained for the glass/epoxy box beam with lower stiffness (Fig. 20). This implies that the nonlinear induced strain effect on smart composite box beams is closely related to the stiffness of the primary structure. The lower the stiffness, the higher is the nonlinear induced strain effect.

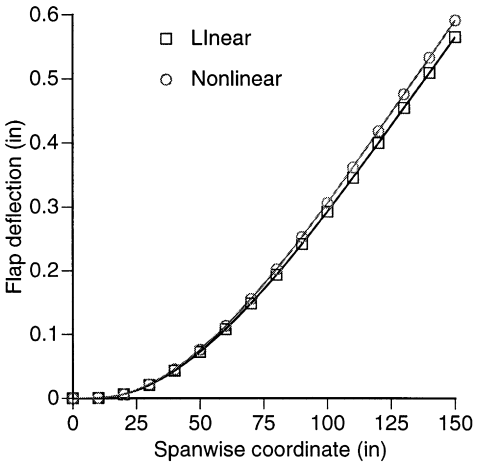

Fig. 19. Nonlinear induced strain effect for box beam made of graphite/epoxy.

6. Concluding remarks

A single-celled composite box beam analysis is developed using a higher order composite laminate theory that accounts for the distributions of shear strains through the thickness of each wall. Individual displacement fields are assumed for each of the four box beam walls. Continuity between the displacement fields is enforced at each of the four corners throughout the thickness of each plate. The resulting solutions of cross-sectional deformations are an approximation of the exact elasticity approach. In this regard, the standard beam degrees of freedom (extension, twist and two bending terms) are not used. The cross section of the beam is fully described by stretching, bending, twisting, shearing and both in-plane and out-of-plane warping. The developed theory is capable of modeling composite box beams of arbitrary wall thickness and will be useful in describing the deformation of moderately thick-walled load carrying members currently being used in rotary wing applications. The following important observations are made:

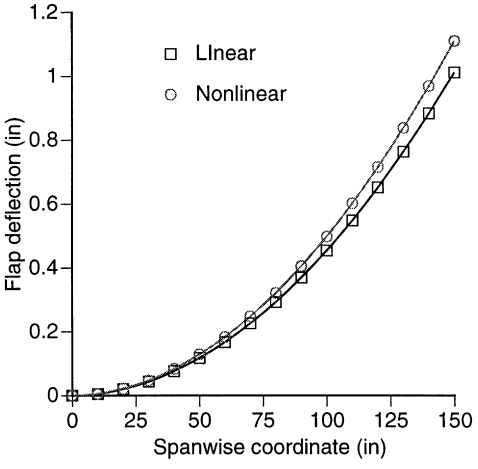

Fig. 20. Nonlinear induced strain effect for box beam made of glass/epoxy.

1. The developed model provides means of accurately evaluating transverse shear deformation and nonlinear induced strain effects.
2. Current solutions agree very well with available experimental data in cases without actuation.
3. For smart box beam with angle ply, conventionally placed actuators control deformations not only in flap plane but also in lag plane and twist.
4. Actuator position affects control authority significantly.
5. Nonlinear induced strain effect on smart composites is closely related to composite material stiffness.

Acknowledgements

The research was supported by the US Army Research Office, Grant number DAAH04-96-1-0163, technical monitor, Dr. Gary Anderson.

Appendix. Details of nonlinear induced strain

Generally, the electro-mechanical coupling between the applied electric field, **E**, the induced strain, **Λ**, the coupling coefficient matrix, **d**, and the strain matrix, $\boldsymbol{\varepsilon}^*$, described in Eqs. (7) and (8) are as follows:

$$\boldsymbol{\Lambda} = \{\Lambda_1 \quad \Lambda_2 \quad \Lambda_3 \quad \Lambda_4 \quad \Lambda_5\}^{\mathrm{T}}, \quad \mathbf{E} = \{E_1 \quad E_2 \quad E_3\}^{\mathrm{T}}$$

$$\mathbf{d} = \begin{bmatrix} 0 & 0 & 0 & d_{15} & 0 \\ 0 & 0 & d_{24} & 0 & 0 \\ d_{31} & d_{32} & 0 & 0 & d_{36} \end{bmatrix},$$

$$\boldsymbol{\varepsilon}^* = \begin{bmatrix} \varepsilon_1 & 0 & 0 & 0 & 0 \\ 0 & \varepsilon_2 & 0 & 0 & 0 \\ 0 & 0 & \varepsilon_3 & 0 & 0 \\ 0 & 0 & 0 & \varepsilon_4 & 0 \\ 0 & 0 & 0 & 0 & \varepsilon_5 \end{bmatrix} \tag{A1}$$

where, ε_i, Λ_i, E_i and d_{ij} are the corresponding components. Since the coupling coefficients, d_{ij}, depend on the actual strain in the actuator as well, they can be expressed in the order of the strain dependency as shown in Eq. (8), in which the components of $\mathbf{d}_0$ and $\mathbf{d}_1$ are

$$\mathbf{d}_0 = \begin{bmatrix} 0 & 0 & 0 & d^0_{15} & 0 \\ 0 & 0 & d^0_{24} & 0 & 0 \\ d^0_{31} & d^0_{32} & 0 & 0 & d^0_{36} \end{bmatrix}$$

$$\mathbf{d}_1 = \begin{bmatrix} 0 & 0 & 0 & d^1_{15} & 0 \\ 0 & 0 & d^1_{24} & 0 & 0 \\ d^1_{31} & d^1_{32} & 0 & 0 & d^1_{36} \end{bmatrix} \tag{A2}$$

According to Crawley and Lazarus [21], these coefficients depend on the corresponding strain components only and they can be identified using functional relationships of the strain versus electric field obtained from experimental data of an unconstrained piezoelectric actuator.

References

[1] McCarthy TR. A new high-order composite theory for analysis and design high speed tilt-rotor blades. PhD dissertation, Arizona State University, 1996.
[2] Hodges DH, Ormiston RA, Peters DA. On the nonlinear deformation geometry of Euler–Bernoulli beams, NASA TP-1566, 1980.
[3] Bauchau OA. A beam theory for anisotropic materials. Journal of Applied Mechanics 1985;52:416–422.
[4] Stemple AD, Lee SW. Finite element model for composite beams with arbitrary cross-sectional warping. AIAA Journal 1988;26(12):1512–1520.
[5] Kosmatka JB, Friedmann PP. Vibration analysis of composite turbopropellers using a nonlinear beam-type finite-element approach. AIAA Journal 1989;27(11):1606–1614.
[6] Rand O. Theoretical modeling of composite rotating beams. Vertica 1990;14(3):329–343.
[7] Wörndle R. Calculation of the cross section properties and the shear stresses of composite rotor blades. Vertica 1982;6:111–129.
[8] Rehfield LW, Atilgan AR, Hodges DH. Nonclassical behavior of thin-walled composite beams with closed cross sections. Journal of the American Helicopter Society 1990;35:42–50.
[9] Chandra R, Stemple AD, Chopra I. Thin-walled composite beams under bending, torsional and extensional loads. Journal of Aircraft 1990;27(7):619–626.
[10] Smith EC, Chopra I. Formulation and evaluation of an analytical model for composite box beams. Journal of the American Helicopter Society 1991;36:23–35.
[11] Reddy JN. A general non-linear third-order theory of plates with moderate thickness. International Journal of Non-Linear Mechanics 1990;25(6):677–686.
[12] Reddy JN. Energy and variational principles in applied mechanics, New York: Wiley, 1984.
[13] Chattopadhyay A, Gu H. A new higher order plate theory in modeling delamination buckling of composite laminates. AIAA Journal 1994;32(8):1709–1716.
[14] Chandra R. Dynamic response of composite beams with induced-strain actuators. SPIE 1994;2190.
[15] Park C, Chopra I. Modeling piezoceramic actuation of beams in torsion. In: Proceedings of the 35th Structures, Structural Dynamics and Materials Conference and Adaptive Structures Forum, Hilton Head, NC, 18–21 April 1994.
[16] Nitzsche E, Breitbach E. A study on the feasibility of using adaptive structures in the attenuation of vibration characteristics of rotor wings. AIAA-92-2452-CP, 1992.
[17] Chen PC, Chopra I. A feasibility study to build a smart rotor: induced-strain actuation of airfoil twist using piezoceramic crystals. In: Proceedings of the SPIE North American Conference on Smart Structures and Materials. Albuquerque, NM, 1993.
[18] Chen PC, Chopra I. Hover test of a smart rotor with induced-strain actuation of blade twist. In: Proceedings of the 36th AIAA/ASME/ASCE/AHS Structural Dynamics and Material Conference and Adaptive Structures Forum, New Orleans, LA. 13–14 April 1995.
[19] Chen PC, Chopra I. Torsion modeling of a smart rotor with induced-strain actuation of blade twist. In: Proceedings of the American Helicopter Society National Technical Specialists' Meeting on Rotorcraft Structures, Williamsburg, VA, 30 October–2 November 1995.
[20] Chattopadhyay A, McCarthy TR. Multidisciplinary optimization of tilt rotor blades using comprehesive composite modeling technique. In: Proceedings of the 53rd Forum of the American Helicopter Society, Virginia Beach, VA, 29 April–1 May 1997.
[21] Crawley EF, Lazarus KB. Induced strain actuation of isotropic and anisotropic plates In: Proceedings of the 30th AIAA/ASME/ASCE/AHS/ASC Structures, Structural Dynamics and Materials Conference, Mobile, AL, 1989:2000–2010.
[22] Tiersten HF. Electroelastic equations for electroded thin plates subjected to large driving voltages. Journal of Applied Physics 1993;74:3389–3393.
[23] Cesnik CES, Sutyrin VG, Hodges DH. Refined theory of twisted and curved composite beams: the role of short-wavelength extrapolation. In: Proceedings of the 35th Structures, Structural Dynamics, and Materials Conference, Hilton Head, SC, 18–20 April 1994:1134–1143.